Tidal Flow Patterns Near A Coastal Headland

Fu E. Tang, Daoyi Chen

Abstract—Experimental investigations were carried out in the Manchester Tidal flow Facility (MTF) to study the flow patterns in the region around and adjacent to a hypothetical headland in tidal (oscillatory) ambient flow. The Planar laser-induced fluorescence (PLIF) technique was used for visualization, with fluorescent dye released at specific points around the headland perimeter and in its adjacent recirculation zone. The flow patterns can be generalized into the acceleration, stable flow and deceleration stages for each half-cycle, with small variations according to location, which are more distinct for low Keulegan-Carpenter number (KC) cases. Flow patterns in the mixing region are unstable and complex, especially in the recirculation zone. The flow patterns are in agreement with previous visualizations, and support previous results in steady ambient flow. It is suggested that the headland lee could be a viable location for siting of pollutant outfalls.

Keywords—Planar laser-induced Fluorescence, recirculation zone, tidal flow, wake flows

I. INTRODUCTION

IN coastal areas, geographical features such as islands and headlands commonly exist. These features could generate recirculation zones, or adjacent areas of low velocity which could trap water, and consequently, any pollutants released in the water. Because coastal areas are highly populated areas, it is important that the water quality of such areas is preserved. In coastal cities, sewage treatment plant outfalls are commonly located into the ocean, disposing of treatment effluents for dilution. If these effluents are not diluted quickly and efficiently, water quality could be compromised.

The authors have carried out studies on flow patterns and pollutant dispersion in headland-generated recirculation zones ([1], [2]). The focus was on steady, uni-directional flow, past a hypothetical headland, which is considered as the worst-case scenario for generating a recirculation zone that traps pollutants. Here, the results of the study on oscillating, or tidal ambient flow is presented. A brief review on field studies and numerical modelling on the field of coastal engineering and island or headland wakes is as follows.

Field studies in this area have been carried out by various researchers, often involving a large area of study and significant funds. Satellite imagery was used in observing coastal flow patterns in a study carried out in the 1980s [3]. A pattern of fringes was presented for island of Jersey using satellite imagery and tracking of drifting buoys [4].

Vorticity measurement was carried out on a front in a California coastline [5]. In [6], the data from the remote sensing survey of the Clyde estuary on the west coast of Scotland was presented. The process of flow separation was demonstrated for the case of an isolated island in a tidal flow. Reference [7] presented a study of the spatial tidal structure around a headland using a shipboard acoustic Doppler current profiler (ADCP). The in-situ velocity was tested by comparing the moored current measurements with velocity measurements from the shipboard ADCP. Reference [8] presented observations of instances of marine pollution using synthetic aperture radar (SAR). In [9], tidal elevations and velocities were modelled using two modelling systems (Princeton Ocean Model and MIKE 3) and compared against field measurements off Singapore's coastal waters. The results indicated that the predicted tidal elevations from the two hydrodynamic modeling systems are almost identical, correlating well to the field measurements, whereas the simulated tidal current velocities or the depth profiles of the velocities from the two model runs may be quite different at the upper layers of the water column. The effects of tidal and non-tidal circulation on a bay (St. Andrew Bay, Florida) during spring and neap tides were studied and presented in [10]. The observed velocities were fitted to diurnal and semidiurnal harmonics separating tidal and sub-tidal motions. The results indicated that the estuary will switch from diurnal tides to semidiurnal tides.

Many numerical or analytical studies have also been carried out, primarily due to lower costs required compared to field studies. In 1987, [11] presented tidal sea mathematical modelling carried out in the Laboratoire National d'Hydraulique (LNF). Falconer has presented island wakes studies on Rattray island ([12], [13]). The island's tidal circulation was modelled and compared with field measurements, aerial observations and satellite imagery [12]. Good agreement was found between the eddy dimensions and circulation strength. Reynolds stresses were also modelled with a semi-empirical turbulence model [13]. The model predicted the size and shape of the eddy well. The free shear layer turbulence was found to be dominant in the mixing zone. Reference [14] studied vortex generation behind a headland in tidal flow using analytical and numerical modelling of the shallow-water equations. Four basic wake regimes were identified: a low Keulegan Carpenter number (KC), high stability parameter (S) which caused vortices generated during the transition to decay quickly, low KC, low S which caused vortex pairing, high KC, high S and high KC, low S which was quasi-steady for both. A comparison of model capabilities on Rattray island was carried out in 1995 [15]. In general the eddy strength was underestimated, due to neglecting free shear layer dynamics as suggested by the authors. Large-scale flow structures have also been receiving

F. E. Tang was with the Victoria University of Manchester, United Kingdom. He is now with the Department of Civil and Construction Engineering, Curtin University Sarawak Campus, CDT 250, 98009 Miri, Sarawak, Malaysia (phone: +60-85-443939; fax: +60-85-443837; e-mail: tang.fu.ee@curtin.edu.my).

D. Chen was with the Victoria University of Manchester, United Kingdom. He is now with the Department of Engineering, the University of Liverpool, United Kingdom (e-mail: Daoyi.chen@liverpool.ac,uk).

World Academy of Science, Engineering and Technology
International Journal of Geological and Environmental Engineering
Vol:6, No:3, 2012

attention ([16], [17]). In [16], the focus was on stability, where a linear stability analysis was performed to determine absolute and convective instability criteria. Mixing was described in [17]. More recent studies include [18], [19], [20] and [21] on various island and headland wakes.

Headland or island wakes and flow patterns have also been studied extensively by modelling in the laboratory. The Reynolds numbers generated in the laboratory should be sufficient in magnitude to represent actual situations. Some laboratory-based studies include [22], [23], and [24]. The authors have also studied the shallow water boundary layer [25]. In [26], wake formation patterns around islands in oscillatory laminar shallow-water flows were presented. In [27], the structure of the eddy shedding was found to be dependent on the KC number. As KC (KC ≈ 15) was increased, the extent of eddy shedding also increased, with regular vortex formation and pairing.

Here, based on Planar Laser-induced Fluorescence (PLIF) flow visualization, the authors aim to describe the flow patterns around and near a hypothetical coastal headland, in oscillating or tidal ambient shallow flow. PLIF flow visualization provides a visual indication of the flow patterns and mass transport of the released tracer (fluorescent dye). With such an understanding, engineering works such as design and siting of sewage treatment plant outfalls could be improved, and damage to the coastal environment minimised. The experimental investigation was carried out at the Manchester Tidal flow Facility, which is capable of generating large-magnitude Reynolds numbers. Attention is paid to the perimeter of the headland, and in its generated recirculation zone.

II. EXPERIMENTAL FACILITIES AND ARRANGEMENT

The details of the experimental facility, the PLIF system and data processing have been presented in [2] and [28]. Thus only the outlines will be given here.

A. Manchester Tidal Flow Facility and the PLIF System

The experiments were conducted in a purpose-built shallow water flume, with full dimensions 11m × 3.3m × 0.2m. A 1:20 plane beach was constructed on one side (See Fig. 1). The headland model consisted of a conical, ellipsoid, head; and a shore connecting section with a triangular cross-section. The bed of the flume and the headland were covered in 5mm median diameter gravel, thus the equivalent roughness, k_s was taken as $2D_g$ according to [29]. To create the tidal flows for the experiments, a uni-directional variable speed pump, and an arrangement of valves connected to both ends of the flume was employed. The valves were opened and closed alternately to create tidal flows. To change the direction of the flow, the state of the valves was changed by a PC housed D/A board and a sinusoidal voltage input. A computer program was written to control the voltage inputs, state of valves, and tidal periods.
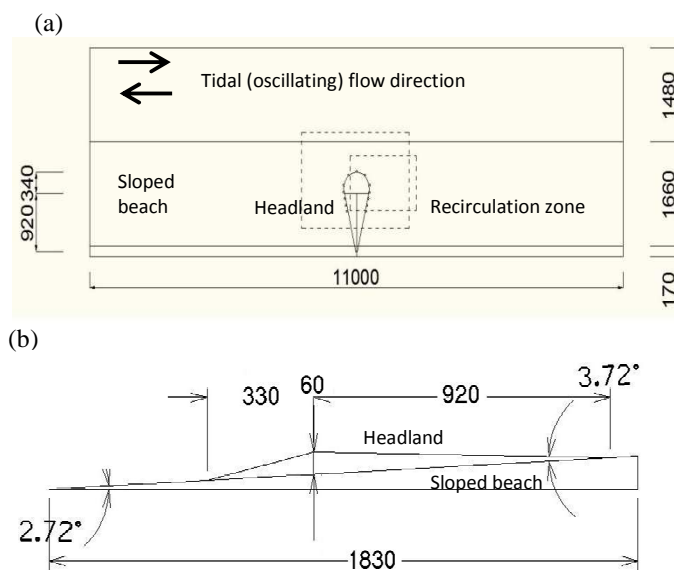
(a)

(b)

Fig. 1 Schematic diagram of the experimental set-up (a) flume and headland (b) side view of headland model and sloped beach. All dimensions in mm. Rectangles (with broken lines) over headland indicate field of view for experiments with high spatial variability (large rectangle) and low spatial variability (small rectangle) relative to flume and headland model

To synchronize the visually observed flow with the state-change of the valves, tidal marking was performed. To mark one point in each half cycle of the tidal period, the state-change signal of the four valves was extracted and indicated by an LED which was brought within the field of view of the camera, which recorded the images.

The PLIF technique is based on the photoluminescence of a fluorescent solution. Reference [30] introduced this non-intrusive method to measure turbulent fluctuations of solute concentration. References [31] and [32] have presented island wake flows and shallow water bounded plane jets featuring the use of the PLIF technique. Reference [33] studied headland wakes using PLIF.

In the experimental set-up here, the fluorescent dye used was Rhodamine-B, released by means of a steel tube submerged in the water, and pumped with a peristaltic pump. A piece of sponge was used to damp the release of the dye, to avoid initial momentum. In [34], submerged round jets were classified to turbulent (Re ≈ 3300 – 3500), transitional (Re ≈ 1600 – 1700) and laminar (Re ≈ 1000). According to the study, turbulent jets exhibited stronger mixing characteristics with considerably smaller decay rate of centreline velocity, compared to laminar jets. Since the velocity of the jet of released dye was minimised in this experiment, it is considered that the effect of the initial conditions are minimised.

A 5W argon laser was used, together with a laser scanner to produce the laser sheet of thickness 2mm. The laser scanner was an 8-faceted diamond turned polygon mirror, which was attached to a level gauge together with its housing, enabling it to be moved up and down a scale. An optical colour glass filter was used to filter out the reflected laser light and retain the emission fluorescence. This filter was attached to the front

World Academy of Science, Engineering and Technology
International Journal of Geological and Environmental Engineering
Vol:6, No:3, 2012

of the camera lens to eliminate the reflected laser light. For capturing the images, a high performance monochrome CCD camera was used. The camera was attached to the roof of the enclosure, about 2.5m from the surface of the flume. To obtain images with high spatial resolution, an 8.5mm lens was used. For digitising the images, a monochrome frame grabber board was used. The grabber produced images with 576×768 pixels, with a greyscale value ranging from $0 - 256$ for each pixel. The area covered is about $1.5m \times 2m$, using the 8.5mm lens.

To enhance the images and improve their appearance, image processing was automated with MATLAB programs. Thresholding and mean (low-pass) filtering were carried out. More details are presented in [28]. To finish, the images are cropped, and a specially-designed, non-linear greyscale colour scheme was added to the images to improve their appearance.

B. Discharge Positions and Experimental Tests

To study the pollutant flushing and flow patterns of the shallow water region near the coastal headland, the experiment was carried out with dye discharged around the perimeter of the headland, and within the headland-generated recirculation zone. Previous studies in steady, ambient flow were carried out with the same discharge points around the perimeter of the headland, and recirculation zone ([1], [2]).

Discharge points around the headland perimeter were located symmetrically around both the left and right sides of the headland (see Fig. 2). From previous studies ([1], [2]), the areas as the current flows past the headland can be divided into the free stream (unobstructed, free and high velocity flow), near shore region (very low velocity, located near the shore and obstructed to incoming flow by the headland) and mixing region (transition between main current and near shore region). The discharge points are located to visualise flow patterns in these areas; where R1, R2, L1, and L2 are nearest to the shore, and indicate behaviour in a bight, at a coastal shoreline; R3, R4, R5, L3, L4 and L5 are in the mixing region; and R6, C, and L6 are near the toe of the headland model and indicate behaviour near the free-stream flow.
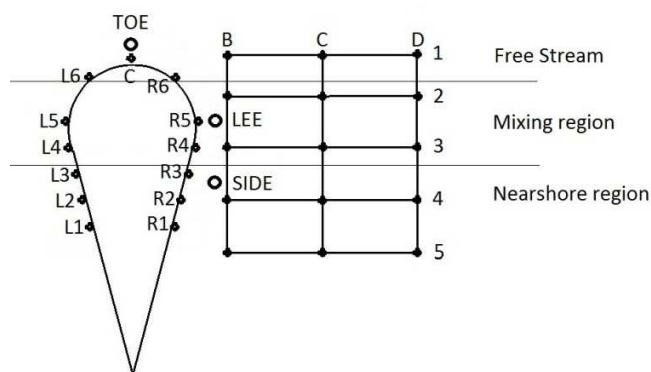

Fig. 2 Schematic diagram of discharge points around the perimeter of the headland and recirculation zone.

To study the recirculation zone systematically, the recirculation zone was divided into a grid (Fig. 2), with columns B, C and D and rows 1 to 5. Dye was discharged at the intersection points of the grid (discharge points B1, C1, D1 for row 1, for example). The furthest column, column D is about two widths of the headland at the widest point of the shore connecting section. This is sufficiently wide to illustrate the behaviour of the recirculation flow [1]. Similarities in flow patterns can be seen across the three columns in each row, were row 1 indicates the main current, rows 2 and 3 the mixing region, and rows 4 and 5 indicate the near shore region.

The test conditions for both the headland perimeter and recirculation zone are presented in Table 1. All experiments were carried out under the same subcritical, turbulent flow condition. The PLIF laser sheet was located 70mm from the bed for all experiments.

TABLE I
FLOW PARAMETERS FOR TIDAL FLOW AT THE HEADLAND PERIMETER AND
RECIRCULATION ZONE

Location	Depth (mm)	Period (s)	Max. free stream vel., (m/s)	Avg. Osc. Re. no.,	Stability para.	KC No.
Perimeter	100	60	0.087	64840	0.245	6.9
Perimeter	108	240	0.102	354090	0.07	32.2
Recirc. Zone	100	60	0.082	57215	0.25	6.5
Recirc. zone	108	240	0.083	229615	0.07	26.1

The oscillatory flow Reynolds number, Re_a is defined as:

$$Re_a = \frac{U_0 a}{\nu} \ , \ a = \frac{U_{0m}}{\omega} \qquad (1)$$

Where U_0 is the free stream velocity, a is the amplitude of fluid particles outside the boundary layer for oscillatory flows, and U_{0m} is the maximum velocity amplitude in the outer region according to:

$$U_0 = U_{0m} \sin \omega t \qquad (2)$$

For values of Re_a reported in this study, U_{0m} is used in place of U_0 in (1).

The stability parameter, S, was calculated according to:

$$S = \frac{c_f D}{H} \qquad (3)$$

Where c_f is the bed-friction coefficient, D is the representative diameter of the headland, estimated at the water level line to be about 0.76m and H is the water depth.

The bed-friction coefficient, c_f is estimated based on [35]. For all bounded flows including open channels, the boundary shear stress is expressed as a coefficient of friction, or c_f where:

$$c_f = \frac{\tau_0}{1/2 \rho U_0} \qquad (4)$$

Where τ_0 is the shear stress between the fluid and the solid surface. Reference [35] presented the effects of varying bed roughness in a water tunnel, and using modified formulas derived by previous researchers plotted a wave friction factor diagram. This diagram was used in the current study to obtain the friction factors for tidal flow over a rough bed.

World Academy of Science, Engineering and Technology
International Journal of Geological and Environmental Engineering
Vol:6, No:3, 2012

The Keulegan Carpenter number, KC, was calculated according to:

$$KC = \frac{U_{0m}T}{D} \qquad (5)$$

where T is the tidal period.

For all experiments, two tidal periods were used, T = 60s and T = 240s. Values of KC and S are calculated for the headland perimeter and headland-generated recirculation zone as above, in Table 1. For any tidal period the flow velocity is a sinusoidal variation (Fig. 3). For each tidal period, to illustrate the flow sequence a total of 24 frames were digitized, covering each phase of the tidal period. Therefore, for a tidal period of 60s, the time interval between two images is 2.5 seconds, and for 240s period, the time interval is 10 seconds. In all the tidal sequences the first half cycle was defined as the movement westward as seen on the image.
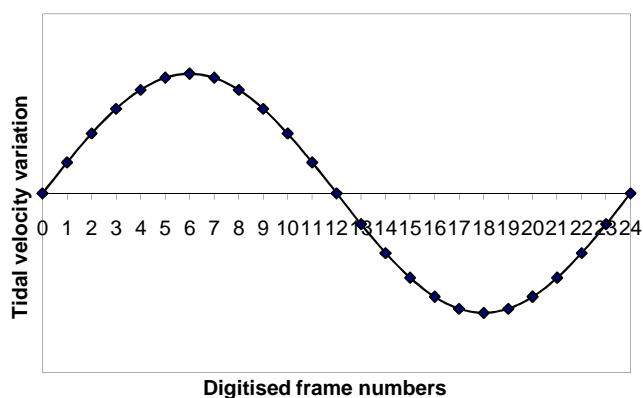

Fig. 3 Schematic representation of tidal velocity variation against digitised frame numbers

III. RESULTS

The generalized flow patterns for both the low KC and high KC cases, pertaining to both discharge locations are shown in Table II.

TABLE II
GENERALIZED TIDAL FLOW PATTERNS

Period (s)	Frame number	Observations
60	1 – 6	Start of movement westward, acceleration, and development of a stable dye plume
	7 – 12	Deceleration of movement and impending direction change. Direction change occurs for some test cases
	13 – 18	Direction change to eastward has occurred, adjustment and acceleration of movement, and development of a stable dye plume
	19 - 24	Deceleration of movement and impending direction change
240	1 – 3	Acceleration of movement westward
	4 – 9	Rapid and stable movement westward
	10 – 11	Deceleration of movement
	12	Transition
	13 – 16	Acceleration of movement eastward
	17 – 21	Rapid and stable movement eastward
	22 - 24	Deceleration of movement and impending direction change

From experimental observation, the flow patterns for both the low KC and high KC cases can be generalised into the acceleration, stable flow and deceleration stages for both half cycles. Variation occurs according to the position of discharge, and is more apparent for the low KC case. For the high KC case the flow patterns were remarkably similar regardless of discharge position. For discharge at the near shore region of the headland perimeter in low KC tidal flow, the released dye plume formed an anticlockwise vortex that was quickly disintegrated during acceleration (further details in Section A). Another anticlockwise vortex was formed during deceleration and disintegrated when the flow direction changes. Accumulation of the released dye occurred, in particular for high KC flow, near the lee of the headland. For discharge points at the mixing region, the anticlockwise vortex as described above was distorted and appears somewhat flattened. This may be due to the increased ambient velocity. Further details on flow patterns in the mixing region are presented in Section B.

For the high KC case, the occurrence of vortices was not prominent throughout the flow visualizations, as compared to the low KC case. Clockwise vortices were seen at the mixing region, at R3, R4 and R5. These vortices occurred during the transition stage, and correspondingly for L3, L4 and L5 anticlockwise vortices were seen during the first acceleration (first half-cycle).

At the recirculation zone, due to the generally low ambient velocity, the flow patterns were complicated. However, similarities were seen for flow patterns across the same row, with some small timing differences observed. The flow patterns in row 1 consisted of simple eastward and westward movement. Flow patterns at row 2 and 3 were complicated and unstable (an example for discharge at B2 is presented in Section C). It is suggested that this is because row 2 and 3 were located within the mixing region, and were affected by the recirculatory eddy. For both rows, for the low KC case, vortices were apparent. However for the high KC case, the occurrence of vortices was less distinct. Unstable flow patterns were also seen for row 4 for both low KC and high KC cases. For row 5, initial accumulation of the released dye was seen, with indistinct flow patterns for both low KC and high KC cases.

Further details on the flow patterns are described in the following three sections, which are mainly focused on the low KC case. Regions of interest include the near shore region for the headland perimeter, and mixing regions for both the headland perimeter and recirculation zone, due to observations of trapping, and complex flow patterns.

A. Discharge around the Headland Perimeter (Near shore region, discharge positions R1 and L1)

For low KC conditions, in frames 1 – 2 the movement started (a typical tidal cycle for dye discharge at R1 is shown in Fig. 4), and an anticlockwise vortex formed in frames 3 – 4, and disintegrated in frame 5. Stable movement westward is observed with a well-formed dye plume from frames 5 to 9. However, the plume changes its angle by as much as 15° to 20° from the horizontal, corresponding to changes in the ambient velocity. In particular, deceleration of the ambient flow is indicated by the instability of the plume. By frames 10 and 11,

World Academy of Science, Engineering and Technology
International Journal of Geological and Environmental Engineering
Vol:6, No:3, 2012

the ambient flow has decelerated and an anticlockwise vortex was formed. While transitioning in frame 12, this vortex remained westwards of the headland, and disintegrated in frames 13 – 15, becoming entrained and dispersed into the flow eastwards (frame 14, Fig. 4). Significant accumulation of the released dye near the discharge point is also seen. In real life situations, if the accumulation of such released pollutants occurs, the water quality of the region may be affected. While the eastward flow is stabilising, the accumulated dye mass is observed to travel towards the main current in frames 16 – 18, while the residual masses of dye from the previous half cycle was dispersed off the field of view by frame 19. Movement towards the free stream is observed in frames 20 to 23, with the start of a new cycle indicated in frame 24.
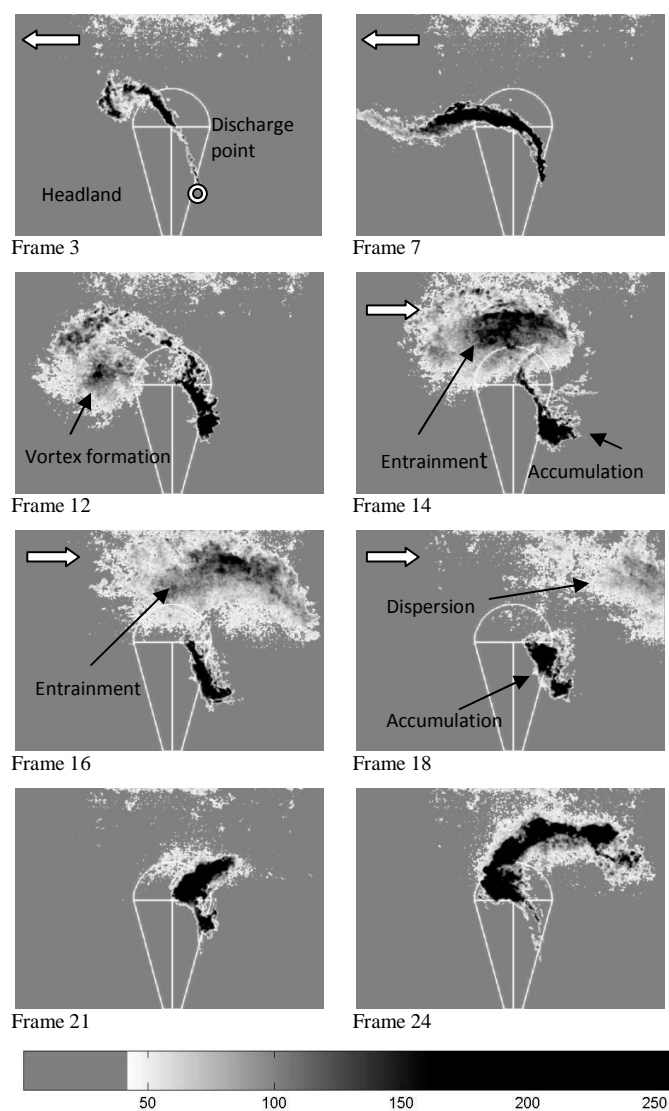
presented in Table 2. Here, some developments for dye discharge at R5 and L5 (low KC case) are shown in Fig. 5.

For the low KC case, dye discharge at both R5 and L5 showed a common vortex, opposed in direction, for both points during the transition stage that was not seen previously (Fig. 5). For discharge at R5, stable westward flow was indicated by the dye plume in frames 4 – 9, and deceleration occurred in frame 10. Some accumulation of released dye was seen at the discharge point in frame 11, and as shown in Fig. 5 a clockwise vortex was seen in frames 12 and 13. The plume was established and moved towards the free stream in frames 14 – 17, and deceleration started in frames 18 – 19. Another clockwise vortex can be seen in frames 20 – 21, and disintegrated in frames 22 – 23. The new period started in frame 24. For L5, the initial anticlockwise vortex was successfully formed in frames 1 and 2, and followed by the dye plume developing and establishing itself in frames 3 – 5. Deceleration started from frame 6 – 8, and in frames 9 – 10 a small anticlockwise vortex was seen (Fig. 5). Transition occurred in frame 11, and from frames 12 – 17 movement eastward was seen. From frames 18 and 19 deceleration started and the residual dye mass was out of view. The plume disintegrated by frame 23.
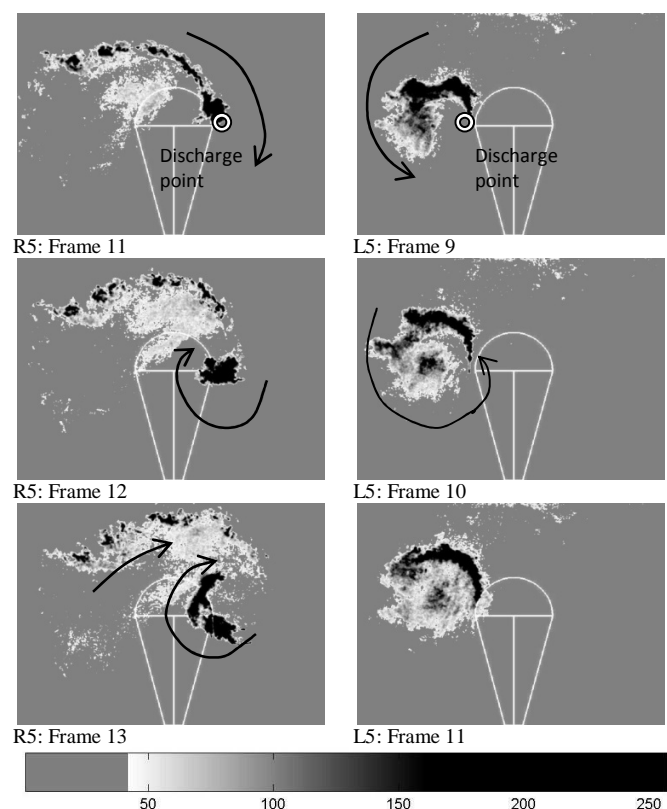

Frame 3 Frame 7
Frame 12 Frame 14
Frame 16 Frame 18
Frame 21 Frame 24

Fig. 4: PLIF images of dye concentration distribution for dye discharge at R1, tidal flow (KC = 6.9, T = 60s). White arrows on top left corner indicate eastward or westward ambient flow

B. Discharge around the Headland Perimeter (Mixing region, discharge positions R5 and L5)

In this region, the evolution of the tidal flow is similar to the near shore region and conforms to the flow patterns

R5: Frame 11 L5: Frame 9
R5: Frame 12 L5: Frame 10
R5: Frame 13 L5: Frame 11

Fig. 5 PLIF images of dye concentration distribution for dye discharge at R5 and L5, tidal flow (KC = 6.9, T = 60s), showing vortices of opposite direction during second acceleration. All curved arrows indicate flow movement

C. Discharge in the Headland-generated Recirculation Zone (Mixing region, discharge positions B2, C2 and D2)

Flow patterns for B2 (low KC case) are presented in Fig. 6. Complicated flow patterns are observed in the second half

Open Science Index, Geological and Environmental Engineering Vol:6, No:3, 2012 publications.waset.org/2590.pdf

World Academy of Science, Engineering and Technology
International Journal of Geological and Environmental Engineering
Vol:6, No:3, 2012

cycle. It is suggested that the erratic flow visualizations observed are due to the velocity instability of the area, as observed earlier (Chen et al. 2003, 2005). For B2 (Fig. 6), two clockwise vortices were seen within the duration of frames 15 – 21. Starting in frames 15 – 17, a clockwise vortex was formed from the adjacent-residual dye (residual dye masses from the previous half cycle that remained within the field of view) as the flow direction changed. This vortex increased in size during the duration of frames 15 – 17. In frame 17 and 18, another clockwise vortex, which was formed from distant-residual dye (residual dye masses that have moved away from the field of view) is seen next to the previous adjacent-residual dye vortex (Fig. 6), forming a complicated dye plume. Both clockwise vortices and dye plume moved away as a high concentration dye mass in frame 19, while minor vortical movement was observed at the discharge point. These patterns disintegrated over frames 22 – 23 as the flow decelerated, and by frame 24 movement westward started. For the high KC case, a clockwise vortex appeared during the transition in frame 13, similar to the low KC case. This vortex was also seen for both C2 and D2, for both high and low KC cases.
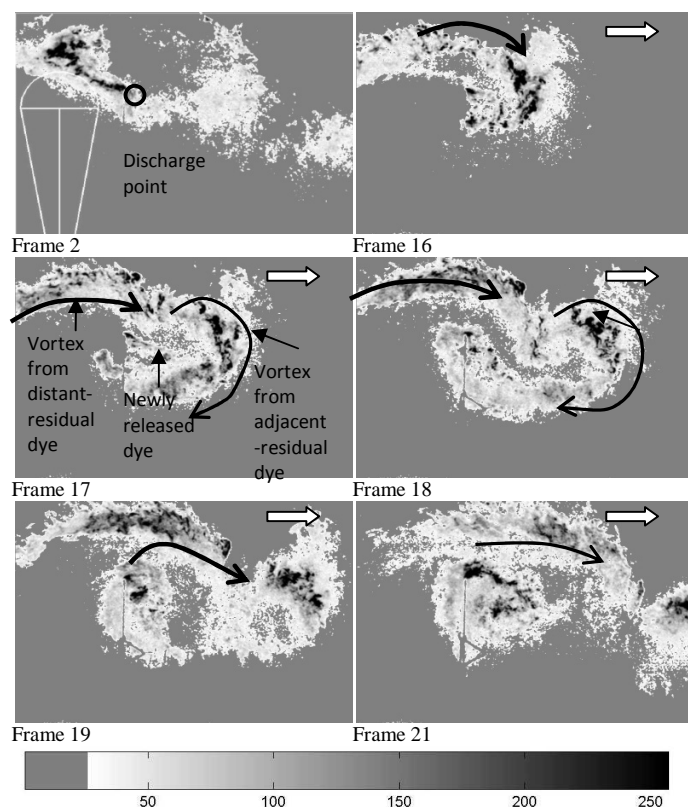

Fig. 6 PLIF images of dye concentration distribution for dye discharge at point B2, tidal flow, (KC = 6.9, T = 60s). All curved arrows indicate movement of residual dye. White arrows on top right corner indicate eastward or westward ambient flow

D. Flow Visualization with Methylene Blue Dye

Lloyd's previous experiments at the UK Coastal Research Facility (UKCRF) had visualised flows with complicated flow patterns and vortex pairing behaviour ([27], [36]). In addition, Lloyd had performed some simple dye visualization experiments at the head of the headland at MTF as in the current study using methylene blue dye. The results obtained in this earlier study were compared with the current PLIF visualization results. Table III lists the flow parameters for these previous experiments.
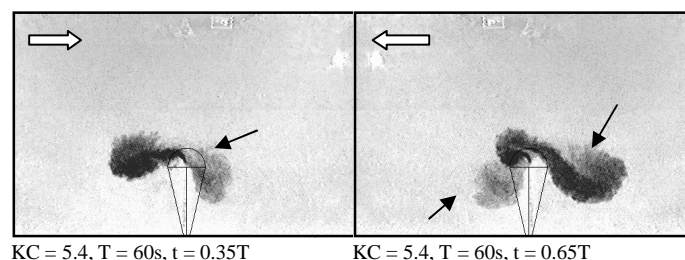
TABLE III
FLOW PARAMETERS FOR METHYLENE BLUE DYE FLOW VISUALIZATION EXPERIMENTS
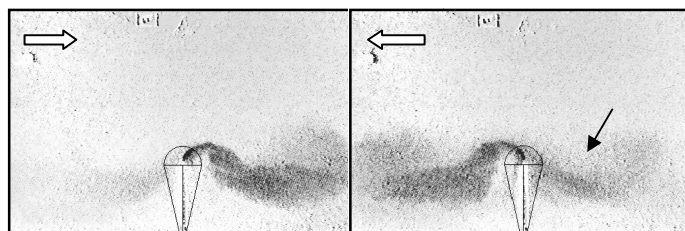
Period (s)	Depth (mm)	Max. free stream vel. (m/s)	Roughness factor (m)	Avg. Osc. Re. No.	KC No.
60	98	0.035	0.01	10130	5.4
60	98	0.059	0.01	28980	9.1
60	98	0.141	0.01	166566	21.7

It was observed that the plume formed with vortices for the low KC case, but no vortices were observed for the high KC case. This is similar to the current PLIF experiments, where vortices were distinct for the low KC case. No instances of accumulation of released dye were observed. This is probably due to the different discharge position, where the methylene blue dye was discharged from the apex of the headland.

For the low KC case (KC = 5.4 in Fig. 7), the flow patterns for both methylene blue dye visualizations were very similar. Due to the low ambient velocity, residual dye was left behind when the flow changed direction (Fig. 7). The span of the movement of dye was about 1 – 2 widths of the headland on either side. At the end of the period residual dye remained at both sides of the headland. Increasing the KC to 9.1 resulted in a similar flow pattern but the visible span of the movement was about 3 – 4 widths of the headland from its centreline. At the end of the first period the residual dye on either side of the headland was symmetrical. For the high KC case (Fig. 7) flow behaviour was similar. The released dye was swept onto the shoreline due to the faster velocity. This occurred during the corresponding half-cycle (i.e. sweeping on eastern shore on eastern half-cycle). However, little dye was entrained.

From the available data for MTF (this current study and Lloyd's early results), the visualizations did not indicate any pairing behaviour. It is suggested here that the absence of pairing behaviour compared with the UKCRF was perhaps due to other reasons, such as bed roughness. The relative bed roughness at UKCRF is 2% while at MTF it is 5%. The vortex pairing may be suppressed by a high relative roughness at MTF (relative roughness here defined by ratio of gravel size to water depth). Also the state of the flow generated at MTF tended to be between transitional to rough turbulent (according to the wave friction chart, [35]) whereas flows at UKCRF were mainly rough turbulent.

KC = 5.4, T = 60s, t = 0.35T   KC = 5.4, T = 60s, t = 0.65T

World Academy of Science, Engineering and Technology
International Journal of Geological and Environmental Engineering
Vol:6, No:3, 2012

| KC = 21.7, T = 60s, t = 0.35T | KC = 21.7, T = 60s, t = 0.85T |

Fig. 7 Images of dye visualization with methylene blue dye, KC = 5.4 and 21.7, T = 60s. White arrows on top left corner indicate eastward or westward ambient flow. Black arrows indicate residual dye

IV. DISCUSSION

The results of this experiment form a component of a study on flow patterns and pollutant dispersion or trapping in the region near and around a hypothetical headland. The results of the study, including the image processing techniques developed, serve to assist the design and siting of marine sewage outfalls, and aid understanding of the dispersion of sewage effluents in tidal waters with geographical features such as headlands and islands. Marine sewage outfalls may be the main means of disposal in coastal cities. For real life projects, further modeling work may be necessary to account for complex geographical features and coastline bathymetry.

In this study, for the experiments to become feasible, distorted scales were used for water depths and headland geometry. In a real life situation, the water depth in such areas is expected to be of the order of 10 m but, the headland dimensions could be of the order of up to 10^2 or 10^3 m. High experimental flow velocities ensure sufficiently high Reynolds numbers for the ambient flow.

In real situations, released pollutants that are entrained into the surrounding flow could also affect the water quality of the area. To observe the potential of the ambient tidal flow for trapping entrained dye, after the dye release was stopped, the dispersion of the residual dye was observed. In low KC ambient flow, the shorter time period allowed more residual dye to circulate in the region. Most of the residual dye was entrained in the flow in the first tidal cycle after dye discharge was stopped. About three to four tidal periods were needed to disperse the dye mass, with significant decrease in the dye concentration by the second tidal period. The longer tidal period of 240s for the high KC case significantly cut short the number of tidal periods needed to disperse the dye (½ to 1 tidal period), despite more dye in volume being discharged for the 240s period. This indicates that the entrainment of pollutants in tidal ambient flow is not significant, in both high and low KC cases.

The authors have conducted experiments with the same hypothetical headland, in steady ambient flow, to study pollutant dispersion in the headland-generated recirculation zone and also around its perimeter. Uni-directional steady flow is taken as the worst case scenario for pollutant trapping in the headland generated recirculation zone. The previous study of the region near a headland in steady flow has indicated the roles of the lee of the headland, and the recirculatory eddy in conveying the released pollutants to be dispersed in the free stream. In brief, the lee of the headland seems to act as a station for dye discharged in the regions nearest to the shore to stagnate, before being dispersed into the free stream. This was observed for steady flow experiments conducted for both the headland-generated recirculation zone, and around its perimeter. As for the recirculatory eddy, it functions to convey the residual dye (after discharge is stopped) back into the recirculation zone, but it also conveys the residual dye to be mixed and diluted at the free stream. The recirculatory eddy is generated from flow separation at the tip of the headland, and recirculates adjacent to the headland, within the recirculation zone as shown in Fig. 2.

The results in this current study complement the results of the steady flow experiments. From the steady flow experiments, which was carried out with the same discharge points around the perimeter of the headland and in its recirculation zone, the recommendation for siting of pollutant outfalls was point Bb (in the middle of B1 and B2) for discharge in the recirculation zone, and R5 or L5 for discharge around the headland perimeter (see Fig. 2). As the current results have indicated that flow patterns at rows 2 and 3 are complex, and due to the proximity of Bb to row 2, thus it seems logical to consider R5 or L5 rather than Bb. By siting the outfalls as near as possible to the shore, and as near as possible to the border between the recirculation and mixing zones, trapping of released pollutants and possible pollution is avoided, while ensuring low costs since it will not be necessary to construct the outfall far into the ocean.

To illustrate further, selected images of dye plumes from discharge around the headland perimeter are superimposed on a single image. The image (Fig. 8) is produced with superimposed dye plumes taken at different discharge points at the same phase. Fig. 8 shows the dye plumes for both the high and low KC cases at the perimeter of the headland. It is seen that for dye discharged within the entire recirculation zone up to the mixing region (R1 – R4, L1 – L4), the dye plume developed an anticlockwise vortex towards the recirculation zone generated downstream. However, for dye discharged at the toe area, the plume seemed to move normal to the shore towards the free stream. Thus a boundary for the recirculation zone can be estimated as seen from Fig. 8. The dye plume from point R5 seems to indicate this boundary itself, for both the high and low KC cases. Thus the results indicate that dye discharge at the mixing region, at point R5 or L5, is most economic, and reinforced the siting recommendation from the steady flow experiments.
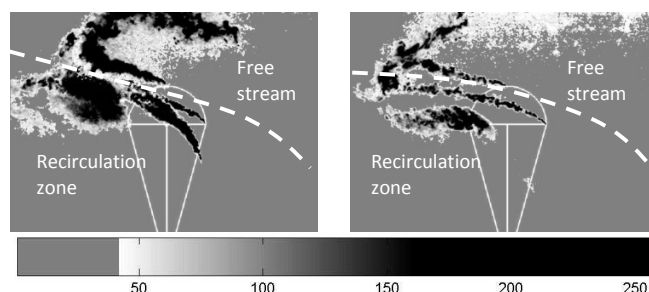

Fig. 8 Superimposed PLIF images of dye plumes for dye discharge at discharge points within the recirculation zone and in the free stream for both low KC and high KC cases. Dashed line indicates estimated position of recirculation zone.

V. CONCLUSION

The flow patterns for both the high and low KC cases can be generalized into stages, which include the acceleration, stable flow and deceleration stages for both half cycles. Variation occurs according to the position of discharge, and is more apparent for the low KC cases. For high KC cases, the flow patterns were remarkably similar regardless of discharge position. For discharge in the recirculation zone, flow patterns at rows 2 and 3 were unstable and complex. This is due to the transitional flow velocities in the mixing region between the recirculation zone, the rapid currents in the free stream.

At the headland perimeter, for points nearest to the shoreline (R1 – R4, L1 – L4), the released dye plume moved around the headland to the opposite side of discharge, and formed an anticlockwise vortex that was quickly disintegrated during acceleration. Another anticlockwise vortex was formed during deceleration and disintegrated when the flow direction changes. Accumulation of the released dye was seen near the lee of the headland for both high and low KC cases. This supports the previous finding that the lee of the headland seems to be a location for the released dye to gather before being dispersed in the free stream. Thus, in real life situations, it is important to monitor the water quality at the lee of the headland.

At the recirculation zone, the flow patterns exhibited similarity on the same row, with some small timing differences. Flow patterns for discharge in row 1 were simple and symmetrical. Flow patterns for discharge at rows 2 and 3 were unstable and manifested complicated dye plumes. For both rows, for the low KC case, movement of dye plume normal to the shoreline was apparent, but not visualized for the high KC case. Some unstable flow patterns were also seen at row 4 for both high and low KC cases. For row 5, flow patterns were indistinct for both high and low KC cases.

The experimental results compliment the authors' previous experiments on pollutant dispersion in the recirculation zone and perimeter of the headland in steady, ambient flow. Due to the complicated nature of the flow in the mixing region as shown here, it is recommended that pollutant outfalls be located at the lee of the headland, to minimize costs of construction in the ocean.

ACKNOWLEDGMENT

REFERENCES

[1] D., Chen, F. E. Tang, C. Chen, "PLIF study of pollutant trapping and 3-D plume structures in recirculation zones around a headland: steady and tidal currents", *In Proc. of the Int. Symp. on Shallow Flows,* ASCE, Holland, 2003

[2] D. Chen, F. E. Tang, C. Chen, "Pollutant trapping at a coastal headland", *J. of Waterway, Port, Coastal and Ocean Eng.,* vol. 131, no. 3, pp. 98-114, 2005

[3] L. Loubersac, "Application of high resolution satellite data in the observation of coastal environment. The case of SPOT simulations within the framework of ecological survey of Brittany coasts". *Special publication, European Space Agency,* 1983

[4] R. D. Pingree, G. T. Mardell, L. Maddock, "Tidal mixing in the channel isles region derived from the results of remote sensing and measurements at sea". *Estuarine, Coastal and Shelf Science,* vol. 20, pp. 1 – 18, 1985

[5] T. F. Duda, and C. S. Cox, "Vorticity measurement in a region of coastal ocean eddies by observation of near inertial oscillations", *Geophys. Res. Lett.*, vol. 14, no. 8, pp. 793-796, 1987

[6] P. A. Davies, L. A. Mofor, "Observations of flow separation by an isolated island". *Int. J. of Remote Sensing,* vol. 11, no.5, 1990

[7] W. R. Geyer, R. Signell, "Measurements of tidal flow around a headland with a shipboard acoustic doppler current profiler". *J. of Geophys. Res.,* vol. 95, no. C3, 1990

[8] M. Gade, W. Alpers, "Using ERS2-SAR images for routine observation of marine pollution in European coastal waters". *The Sci. of the Total Environment.* vol. 237/238, pp. 441 – 448, 1999

[9] Q. Y. Zhang, 2006. "Comparison of two three-dimensional hydrodynamic modeling systems for coastal tidal motion". *Ocean Eng.* vol. 33. pp. 137 – 151, 2006

[10] P. L. Murphy, A. Valle-Levinson, "Tidal and residual circulation in the St. Andrew Bay system, Florida". *Continental Self Research,* vol. 28. pp. 2678 – 2688, 2008

[11] Y. Coeffe, S. Courtier, B. Latteux, "Tidal sea mathematical modeling: current applications and future developments". *Coastal Eng.,* vol. 11, pp. 479 – 511, 1987

[12] R. A. Falconer, E. Wolanski, L. Mardapitta Hadjipandeli, "Modelling tidal circulation in an island's wake". *J. of Waterway, Port, Coastal and Ocean Eng.,* vol. 112, Iss. 2, pp. 234-254, 1986

[13] R. A. Falconer, L. Mardapitta Hadjipandeli, "Bathymetric and shear stress effects on an island's wake: a computational model study". *Coastal Eng.,* vol. 11, pp. 57 – 86, 1987

[14] R. P. Signell, W. R. Geyer, 1991. "Transient eddy formation around headlands". *J. of Geophys. Res.,* vol. 96, no. C2, 1991

[15] D. Galloway, E. Wolanski, B. King, "Modelling eddy formations in coastal waters: A comparison between model capabilities". *Proc. of the conf. on Estuarine and Coastal Modelling,* 1995, pp. 13 – 25.

[16] S. A. Socolofsky, G. H. Jirka, "Large-scale flow structures and stability in shallow flows". *J. of Environmental Eng. Sci.* vol. 3, Iss. 5, pp. 451 – 462, 2004

[17] G. H. Jirka, "Large-scale flow structures and mixing processes in shallow flows". *J. of Hyd. Res.* vol. 39, Iss. 6, pp. 567 – 573, 2001

[18] C. Dong, J. C. McWilliams, "A numerical study of island wakes in the Southern California Bight", *Continental Shelf Research,* vol. 27, no. 9, pp. 1233-1248, 2007

[19] M. J. Alaee, C. Pattiaratchi, G. Ivey, "Numerical simulation of the summer wake of Rottnest Island, Western Australia", *Dynamics of Atmospheres and Oceans,* vol. 43, no. 3-4, pp. 171–198, 2007

[20] I. M. Brooks, S. Soderberg, M. Tjernstrom, "The turbulence structure of the stable atmospheric boundary layer around a coastal headland: aircraft observations and modeling results", *Boundary Layer Meteorology,* vol. 107, pp. 531-559, 2003

[21] P. F. Coutis, J. H. Middleton, "The physical and biological impact of a small island wake in the deep ocean". *Deep Sea Research I.* vol. 49, pp. 1341 – 1361, 2002

[22] O. Leuchter, J. L. Solignac, "Experimental investigation of the turbulent structure of vortex wakes". *Proc. of the 4th Int. Symp. on Turbulent Shear Flows*, 1985, pp. 156 – 168.

[23] P. Menzel, F. Huttmann, M. Brede, A. Leder, "Experimental investigations of mixing processes in the wake of a circular cylinder in stratified flows". *Proc. of the Conf. on Multiphase flow: The Ultimate Measurement Challenge*, 2007, pp. 122 – 127.

[24] C. F. v. Carmer, A. C. Rummel, G. H. Jirka, "Mass transport in shallow turbulent wake flow by planar concentration analysis technique". *J. of Hyd. Eng.* vol. 135, no.4, pp. 257 – 270, 2009

[25] D. Chen, C. Chen, F. E. Tang, P. Stansby, M. Li, "Boundary Layer Structure of Oscillatory Open-Channel Shallow Flows over Smooth and Rough Beds", *Experiments in Fluids,* vol. 42, no. 5, pp. 719-736, 2007

[26] P. M. Lloyd, P. K. Stansby, D. Chen, "Wake formation around islands in oscillatory laminar shallow-water flows", *J. of Fluid Mechanics,* vol. 429, 2001

[27] P. M. Lloyd, P. K. Stansby, "Shallow-water flow around model conical islands of small side slope. I: surface piercing", *J. of Hyd. Eng.,* vol. 23, no. 12, pp. 1057-1068, 1997

[28] F. E. Tang, "Visualization of tidal flow near a coastal headland", *Proc. Of the Marine Waste Water Discharge (MWWD) Conf. 2010, Langkawi, Malaysia,* 2010

[29] J. F. A. Sleath, "Turbulent oscillatory flow over rough beds", *J. of Fluid Mechanics,* vol. 182, 1987
[30] P. N. Papanicolaou, E. J. List, "Investigations of round vertical turbulent buoyant jets". *J. of Fluid Mechanics,* vol. 209, pp. 151 – 190, 1988
[31] Chen, D., Jirka, G.H., "Pollutant mixing in wake flows behind islands in shallow water", *in Proc. of the Int. Symp. on Environmental Hydraulics,* Hong Kong, 1991, pp. 371-377.
[32] Chen, D., Jirka, G.H., "LIF study of plane jet bounded in shallow water layer", *J. of Hyd. Eng.* vol. 125, no. 8, pp. 817-826, 1999
[33] D. G. MacDonald, G. H. Jirka, "Characteristics of headland wakes in shallow flow", *In Proc. of the Congress of the IAHR,* Netherlands, 1997, pp. 88 – 93.
[34] L. P. Xia, K. M. Lam, "Velocity and concentration measurements in initial region of submerged round jets in stagnant environment and in coflow", *J. of Hydro-Environment Res.,* vol. 3, no. 1, pp. 21-34, 2009
[35] J.W. Kamphuis, "Friction factor under oscillatory waves". *J. of the waterways, harbors and coastal eng. div.* vol. 101, no. WW2, 1975
[36] P.M. Lloyd, P.K. Stansby, D. Chen, R.A. Falconer, J. Yin, Y. Chen, "Eddy formation around a conical headland in oscillatory shallow-water flow". *Private communication,* 2004